PERGAMON

Chemical Engineering Science 56 (2001) 157–172

Chemical Engineering Science

www.elsevier.nl/locate/ces

Comparison between two- and one-field models for natural convection in porous media

Raúl A. Bortolozzi, Julio A. Deiber*

Instituto de Desarrollo Tecnológico para la Industria Química (INTEC), Güemes 3450-3000, Santa Fe, Argentina

Received 29 October 1999; received in revised form 23 June 2000; accepted 31 August 2000

Abstract

The two-field model (2-F) for natural convection in porous media is studied in relation to the one-field model (1-F), which is the result of the local thermal equilibrium assumption. These models are used to evaluate heat transfer through a porous medium of relatively high permeability contained in a vertical annulus. The conceptual differences between 2- and 1-F models are shown within the context of the theory of mixtures of continuum mechanics. Criteria are generated to determine when the 1-F model can be applied in practical situations as a good approximation, and without introducing errors in the evaluation of the temperature field and wall heat fluxes. This study includes a comparison between the Nusselt numbers obtained from these two models, and also the analysis of local differences between fluid and solid temperatures within the porous cavity. Numerical calculations are carried out for variable porosity, which is modeled either with exponential decaying and damped oscillating functions involving normal distance from the annulus walls. Different correlations for the heat transfer coefficient between solid and fluid phases are analyzed in relation to the 2-F model.

Keywords: Natural convection; Porous media; Theory of mixtures; Two-field model; One-field model; Non-Darcian effects

1. Introduction

The flow and heat transfer in porous media is a subject of technological interest for the design of industrial equipments. Typical examples are catalytic reactors, energy storage units, heat exchangers, thermal insulations, grain storage and solar receiver devices. In addition, there are natural systems formed by different porous media, which are important sources of energy, like geothermal and oil–gas reservoirs. All these systems, and many others, have in common the need of modeling appropriately the flow and heat transfer of Newtonian fluids in a porous medium which, depending on the porosity and permeability values, will show different phenomena. In this sense, several models assigning a temperature field alone to the mixture composed by the interstitial fluid and the solid matrix were proposed and discussed in the literature (see, for example, Cheng, 1978; Whitaker, 1986). These theoretical proposals are designated 1-F models throughout this work and they have been widely used in the literature in the past decade. On the other hand, a few authors used 2-F models where two fields of temperature were required to describe appropriately the heat transfer between solid and liquid phases. For example, Vortmeyer and Schaefer (1974) proposed a one-directional 2-F model for gas flowing by forced convection in a porous medium. To solve this problem, these authors considered that the heat capacity of the gas was negligible against that of the solid and that the second derivative of the solid and fluid temperature fields were equal. They found that under this specific hypothesis, the model was reduced to only one energy balance. This result allowed them to obtain the solid temperature while the gas temperature was calculated through a simple algebraic equation related to the solid temperature field. In a similar context of analysis, Riaz (1977) found an analytic solution of a 2-F model for a one-directional flow. Although simplifying assumptions were introduced in these works, it was found that the solid and fluid temperature fields were in general different from one another, unless specific physical conditions were imposed, like the case in which the heat transfer coefficient between both phases became very high. Later Spiga and

* Corresponding author. Tel.: + 54-42-559174/75/76; fax: + 54-342-4550944.

E-mail address: treoflu@arcride.edu.ar (J.A. Deiber).

0009-2509/01/$ - see front matter
PII: S0009-2509(00)00415-2

Spiga (1981) presented analytic solutions to the transient problem for different initial conditions, with less restrictive hypothesis than those imposed in the work of Riaz (1977). Once more, it was found that the solid and fluid phases had associated different temperature fields in a typical phenomenological situations.

The theoretical progress on this subject was accompanied by a few experimental programs where the local temperature fields were determined in the porous medium. Thus, Wong and Dybbs (1976) carried out temperature measurements with thermocouples at different positions in a porous medium constituted by spheres of uniform diameter, while water was flowing through the interstices. Since the experimental measurements were reported for relatively low fluid velocities, differences between the solid and fluid temperatures were not detected, and hence, these authors concluded that the local thermal equilibrium (LTE) assumption, defined as equal solid and fluid temperatures everywhere in the porous matrix, was rather appropriate for their system.

Although the hypothesis of LTE is good for many applications, it cannot be used in some particular situations that will be analyzed in this work. In fact, other authors carried out studies to show that under certain physical conditions, the solid and temperature fields can differ substantially in specific zones of the porous matrix. In this sense, one has to describe appropriately the heat exchange between the solid and fluid (see, for example, Wakao & Kaguei, 1982; Martin, 1978) which must appear as an extra term in the energy balances of the 2-F model types.

In this context of analysis, Amiri and Vafai (1994) presented a 2-F model for the one-directional flow in a conduit filled with a porous medium. In their model, the balance of momentum included Darcy, Brinkman, Forchheimer, inertial terms (see also, Chen, Chen, Minkowycz, & Gill, 1992; Vafai & Kim, 1995) and the porosity variation near the tube walls (Vafai, 1984). In addition, the energy balances for each phase involved the heat exchange between solid and interstitial fluid. This effect was modeled with the external heat transfer coefficient, which was described with a correlation that comprised the Prandtl and Reynolds numbers. Thus, the internal heat transfer coefficient in the solid was considered negligible. After solving this model numerically with finite differences, the authors obtained a relevant conclusion indicating that the LTE assumption was valid for certain values of dimensionless parameters, which were additionally calculated from the thermophysical properties of the fluid and the morphological characteristics of the porous medium. More recently, a similar problem was solved by Kuznetsov (1997) by means of a perturbation analysis, where the small parameter was the difference between solid and fluid temperatures. In fact, since the asymptotic LTE was valid when these temperatures became very close, the author assumed that this difference was proportional to the fluid velocity and inversely proportional to the heat transfer coefficient between phases.

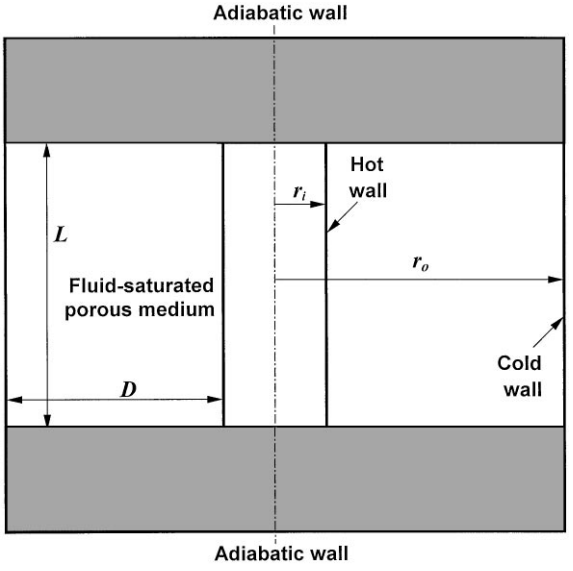

Fig. 1. Annular porous cavity: scales and coordinate system.

When the heat transfer is considered in a porous medium where the fluid moves by natural convection, one finds that classical models reported in the literature use the temperature field of the fluid–solid mixture with the LTE assumption. Under certain conditions of the porous medium to be analyzed later, this proposal is a good approximation to the evidences discussed above, although results show that the way to describe more precisely this type of heterogeneous heat transfer phenomenon is through a 2-F model. This was analyzed in part in the pioneering work of Combarnous and Bories (1975) involving natural convection in a geothermal reservoir. Therefore, the target of our work is to demonstrate quantitatively in the elementary context of the theory of mixtures (Truesdell, 1969; Bowen, 1976) the importance of considering the 2-F model in natural convection, mainly when the permeability of the porous medium is relatively high, and also to show agreements and conceptual differences between 2- and 1-F models. These models are used to evaluate the heat transfer through a porous medium of relatively high permeability contained in a vertical annulus (see Fig. 1).

We show here that the 2-F model can be reduced for many practical situations to the 1-F model. Therefore, conditions at which the LTE assumption is satisfied are presented. The most important differences between models are in fact found in those terms that involve the temperatures of the fluid and solid phases. These terms can be visualized clearly when the compatibility conditions of the theory of mixtures are applied to obtain from

the balances of species, the balance equations of the mixture as a whole (Truesdell, 1969). Proceeding in this way, criteria are generated to determine when a 1-F model can be applied in practical situations as a good approximation, and without introducing errors in the evaluation of the temperature field and wall heat fluxes. This local aspect of the problem is important to be analyzed in general, because the precise knowledge of the temperature field of the solid phase is required in industrial devices where chemical reactions take place within a bed of particles of relatively high permeability.

In this work, a crucial problem also becomes evident in relation to the formulation of the momentum balance of the fluid phase in the porous medium, when the flow field is obtained from either the 2- and 1-F theoretical framework. In fact, for the 1-F model, the driving force of natural convection is proportional to the difference between the fluid temperature that is assumed equal to the solid temperature, and the reference temperature T_r, used to expand the fluid density as function of $(T - T_r)$. Here, T_r is chosen as the arithmetic average between the hot T_h and cold T_c wall temperatures. On the other hand, in the 2-F model, this driving force involves the difference between the *true* fluid temperature T_f and the reference temperature T_r. Therefore, when the LTE assumption is valid, the consistency between 1- and 2-F models is readily obtained and the numerical results validate that either the fluid or solid temperature can be used in the driving force term of the natural convection. This is not the case, when the LTE assumption cannot be applied. In fact, for this particular case, the velocity fields obtained by solving 1- and 2-F models are different from one another, because the driving body forces in each model are, of course, also different. Since the flow field shall be the same for the two models, it is clear that this subject requires still further research to elucidate this physical aspect. In this work, therefore, we propose to study and discuss this problem to find the conceptual relationship between the two ways of modeling natural convection in porous media. This task has to be done taking into account a specific theory as a reference framework to avoid excessive heuristic considerations. Therefore, for this purpose, the theoretical approach and the porous medium considered here are those of our previous work (Deiber & Bortolozzi, 1998) where the 2-F model has already been presented and discussed by using the theory of mixtures (see also Fig. 1).

Throughout this work importance is given to the analysis of numerical calculations carried out for variable porosity, which is modeled either with exponential decaying (Vafai, 1984) and damped oscillating (Martin, 1978) functions involving normal distance from the annulus walls. Since the 2-F model requires to quantify the heat exchange between solid and fluid phases, three different correlations for the interfacial heat transfer coefficient are also analyzed.

2. Framework within the theory of mixtures

The theory of mixtures considers N species, the properties of which are designated with a subscript $\alpha = 1, \ldots, N$ (Truesdell, 1969; Bowen, 1976). Therefore mass, momentum and internal energy of species satisfy local balances as follows:

$$\frac{\mathrm{d}_\alpha}{\mathrm{d}t}\rho_\alpha + \rho_\alpha \nabla \cdot \mathbf{v}_\alpha = 0, \tag{1}$$

$$\rho_\alpha \frac{\mathrm{d}_\alpha}{\mathrm{d}t}\mathbf{v}_\alpha = -\nabla \cdot \mathbf{T}_\alpha + \rho_\alpha \mathbf{g} + \mathbf{m}_\alpha, \tag{2}$$

$$\rho_\alpha \frac{\mathrm{d}_\alpha}{\mathrm{d}t}U_\alpha = -\nabla \cdot \mathbf{q}_\alpha - \mathbf{T}_\alpha : \nabla \mathbf{v}_\alpha - \mathbf{m}_\alpha \cdot \mathbf{v}_\alpha + e_\alpha^T, \tag{3}$$

where density ρ_α, velocity $\mathbf{v}_\alpha$, internal energy U_α and stress tensor $\mathbf{T}_\alpha$ of species α are included. This tensor is assumed to be symmetric here. The only volumetric force is gravity $\mathbf{g}$. In Eqs. (1)–(3), $\mathrm{d}_\alpha(\cdot)/\mathrm{d}t = \partial(\cdot)/\partial t + \mathbf{v}_\alpha \cdot \nabla(\cdot)$ is the species time derivative. Further details are described in the original works. In Eq. (3), $\mathbf{q}_\alpha$ is the flux by heat conduction of species α. In writing Eqs. (1)–(3), it is assumed that chemical reaction and volumetric heat transfer do not occur in the system.

This theory considers the exchanges of momentum $\mathbf{m}_\alpha$ and total energy e_α^T (kinetic plus internal energies) between species with the constraint that the local equations of the mixture are recovered when Eqs. (1)–(3) are summed on α, in order to be consistent with the behavior of the mixture as a whole (see also the basic postulates of the theory of mixtures according to Truesdell, 1969). Therefore, the following compatibility conditions shall be required among the mixture and species properties:

$$\rho = \sum_{\alpha=1}^{N} \rho_\alpha, \tag{4}$$

$$\mathbf{v} = \frac{1}{\rho}\sum_{\alpha=1}^{N} \rho_\alpha \mathbf{v}_\alpha, \tag{5}$$

$$\mathbf{T} = \sum_{\alpha=1}^{N} (\mathbf{T}_\alpha + \rho_\alpha \mathbf{u}_\alpha \mathbf{u}_\alpha), \tag{6}$$

$$\mathbf{q} = \sum_{\alpha=1}^{N} \left[\mathbf{q}_\alpha + \mathbf{T}_\alpha \cdot \mathbf{u}_\alpha + \rho_\alpha (U_\alpha + \frac{1}{2}\mathbf{u}_\alpha^2)\mathbf{u}_\alpha \right], \tag{7}$$

$$U = \frac{1}{\rho}\sum_{\alpha=1}^{N} \left(\rho_\alpha U_\alpha + \frac{1}{2}\rho_\alpha \mathbf{u}_\alpha^2 \right), \tag{8}$$

where ρ, $\mathbf{v}$, $\mathbf{T}$, $\mathbf{q}$ and U are the density, velocity, stress tensor, heat flux and internal energy of the mixture, respectively. In the above equations, $\mathbf{u}_\alpha = \mathbf{v}_\alpha - \mathbf{v}$ is the drift velocity of each uniform phase when heterogeneous systems are considered. $\mathbf{u}_\alpha$ is also designated diffusion

velocity of each species α when a miscible mixture is under analysis.

Also, the following constraints must be satisfied to obtain the local balances of the mixture:

$$\sum_{\alpha=1}^{N} \mathbf{m}_\alpha = 0, \quad \sum_{\alpha=1}^{N} e_\alpha^T = 0 \tag{9}$$

indicating that the momentum and total energy of the whole mixture are neither created nor destroyed in the exchange of these properties among species.

3. 2-F model for the porous medium

Eqs. (1)–(9) can be used to describe the flow and heat transfer of a Newtonian fluid in an undeformable and saturated porous medium by taking $\alpha = f, s$ where f refers to the fluid and s stands for the solid. Thus, $\rho_f = \rho_f^o \varepsilon$ and $\rho_s = \rho_s^o(1-\varepsilon)$, where ε is the local porosity. Throughout this work, superscript o indicates that properties correspond to pure species.

Several additional definitions are next required. Density depends on fluid temperature T_f through $\rho_f^o = \rho_{fr}^o[1-\beta(T_f - T_r)]$, where β is the isobaric thermal expansion coefficient. Since the fluid is Newtonian, the stress tensor is expressed $\mathbf{T}_f = p_f^o \varepsilon \mathbf{I} - \mu_f^o \varepsilon(\nabla \mathbf{v}_f + \overline{\nabla \mathbf{v}_f}^{\mathrm{T}})$. Also, we consider that the other thermophysical properties of fluid and solid are constant, which is a good hypothesis for the porous cavity described in Fig. 1 (Deiber & Bortolozzi, 1998).

The heat fluxes of species in the mixture are defined as

$$\mathbf{q}_s = -k_s \nabla T_s, \tag{10}$$

$$\mathbf{q}_f = -(k_f \mathbf{I} + \mathbf{k}_d)\cdot \nabla T_f, \tag{11}$$

where k_s and k_f are the partial thermal conductivities of solid and fluid in the mixture defined as thermodynamic partial properties (for the basic concept see, for example, Glasstone, 1947) and they shall be functions of thermal conductivities of the pure species as well as bed porosity. Thus, when the mixture is considered ideal these properties are $k_s = k_s^o(1-\varepsilon)$ and $k_f = k_f^o \varepsilon$, where k_s^o and k_f^o are the thermal conductivities of solid and fluid as pure species. The sum of these fluxes is a part of the total flux $\mathbf{q}$, which is calculated from Eq. (7). In the framework of 1-F models, several semiempirical expressions for the effective stagnant thermal conductivity of porous media are available in the literature (Nield, 1991; Prasad, Kladias, Bandyopadhaya, & Tian, 1989) which allow us to defined k_s and k_f. In particular, the correlation of Kunii and Smith (1960) has been found useful in practice. Therefore, one can readily propose for this case, $k_f = k_f^o \varepsilon$ and $k_s = k_s^o(1-\varepsilon) f_c$, where $f_c = (2/3 + a_1/r_c)^{-1}$ so that the sum of these expressions satisfies the effective stagnant thermal conductivity proposed by these authors. The equation for f_c involves the empirical constant a_1, which is calculated through the relation $a_1 = 4.63(\varepsilon - 0.26)(\varphi_1 - \varphi_2) + \varphi_2$, where φ_1 and φ_2 can be obtained as function of the conductivity ratio $r_c = k_f^o/k_s^o$, from a plot presented in Kunii and Smith's work. Of course, for the ideal mixture used in our previous work, one gets a stagnant thermal conductivity $k_m = k_s^o(1-\varepsilon) + k_f^o \varepsilon$ with $f_c = 1$. In this work, the correlation of Kunii and Smith is used as suggested in Nield's work. Nevertheless, in systems where the thermal conductivities of the pure species are relatively close, like the case of water–glass system, the value of k_m obtained with the correlation mentioned above is similar to that of the ideal mixture.

In Eq. (11), $\mathbf{k}_d$ is the thermal dispersion tensor generated by the fluid convective fluctuation in the interstices (Georgiadis & Catton, 1988). This tensor is expressed (see Mercer, Faust, Miller, & Pearson, 1982; Amiri & Vafai, 1994; Howle & Georgiadis, 1994),

$$\mathbf{k}_d = \rho_f^o C_{pf}^o d_p l(n)\mathbf{a}: \frac{\varepsilon(\mathbf{v}_f \mathbf{v}_f)}{|\mathbf{v}_f|}. \tag{12}$$

Since the porous media is considered isotropic, the tensor $\mathbf{a}$ has symmetric properties as described by Scheidegger (1974); thus, $a_{iiii} = a_l$, $a_{iijj} = a_t$, $a_{ijij} = a_{ijji} = \frac{1}{2}(a_l - a_t)$ for all possible permutations when $i = r, z$ in a cylindrical coordinate system (Fig. 1); otherwise, components of $\mathbf{a}$ are zero. In Eq. (12), C_{pf}^o is the fluid heat capacity at constant pressure and d_p is the particle diameter. Also, $l(n)$ is the Van Driest function (Cheng & Hsu, 1986) which considers the damping of fluid fluctuations near the walls and is expressed as

$$l(n) = 1 - \exp\left(\frac{n}{\omega d_p}\right), \tag{13}$$

where n is the perpendicular distance from any wall of the porous cavity and ω is an empirical constant (Cheng & Zhu, 1987).

In relation to Eq. (12) another consideration is useful. In fact, since for the purposes of this work the thermal conductivity ratio r_c and the Darcy number Da were changed within a wide range of values, the Rayleigh number Ra obtained never became greater than 3.5×10^4, to avoid unphysical $\Delta T = T_h - T_c$. This particular situation allowed us to use Eq. (12) with the same value for the longitudinal and transversal components of the dispersivity tensor ($a_l = a_t = a$), i.e. the dispersion effect can be considered isotropic (Bortolozzi & Deiber, 1998). This consideration is applied throughout this work reducing Eq. (12) to the scalar form $k_d = \rho_f^o C_{pf}^o d_p l(n) a \varepsilon |\mathbf{v}_f|$.

The internal energy exchange between species, $e_\alpha = e_\alpha^T - \mathbf{m}_\alpha \cdot \mathbf{v}_\alpha$, is defined (see, for example, Combarnous & Bories, 1975; Amiri & Vafai, 1994),

$$e_s = -e_f = h_{sf} a_v (T_f - T_s), \tag{14}$$

where a_v is the specific surface of the porous medium evaluated from $a_v = 6(1-\varepsilon)/d_p$. This last expression is deduced from geometric considerations (see, for example, Bird, Stewart, & Lightfoot, 1960).

The heat exchange between the interstitial fluid and the particles in the porous medium is still a subject of research and has not been fully elucidated yet (see, for example, Kaviany, 1995). In fact, a single particle in a typical cell of the porous medium exchanges heat with the moving surrounding fluid and also with the neighboring particles that are in direct contact. A simple approach to this problem is to assume that the total heat transfer coefficient describing the heat exchange between phases has associated two resistances (internal and external to the particle). Thus, Eq. (14) involves the heat transfer coefficient h_{sf}, which in this work is evaluated with the following expression (Kuznetsov, 1998) as

$$\frac{1}{h_{sf}} = \frac{1}{h_f} + \frac{l_c}{k_s^o}. \tag{15}$$

In Eq. (15), the value of h_f can depend on the fluid velocity and thermophysical properties according to the following generalized expression:

$$h_f = \psi \frac{k_f^o}{d_p}\left[2 + cPr_f^m\left(\frac{Re_p}{s}\right)^q\right], \tag{16}$$

where $Re_p = \rho_{fr}^o \varepsilon |\mathbf{v}_f| d_p/\mu_f^o$ is the particle Reynolds number and $Pr_f = C_{pf}^o \mu_f^o/k_f^o$ is the fluid Prandtl number. The widely accepted equation of Wakao, Kaguei, and Funazkri (1979) (designated Correlation (a) throughout this work) is obtained from Eq. (16) when $\psi = 1$, $c = 1.1$, $m = \frac{1}{3}$, $q = 0.6$ and $s = 1$; we adopt this correlation to generate our numerical results. Nevertheless, to validate this choice, in the discussion section the numerical predictions involving Correlation (a) are compared with those obtained with Correlation (b) which results by taking $\psi = 1$, $c = 0.6$, $m = \frac{1}{3}$, $q = 0.5$ and $s = 1$ in Eq. (16) (see Bird et al., 1960). In a similar context one can use Correlation (c) suggested by Martin (1978) with $\psi = 1 + [1.5(1-\varepsilon)]$, $c = 0.6$, $m = \frac{1}{3}$, $q = 0.5$ and $s = \varepsilon$.

In Eq. (16), the internal heat transfer coefficient, which involves pure conduction, is treated as a lumped parameter including a characteristic length l_c. This length is estimated to be around $d_p/10$ for spheres (Dixon & Cresswell, 1979; Stuke, 1948). In our previous work (Deiber & Bortolozzi, 1998) $h_{sf} \approx h_f$ was considered as a first approximation for the water–glass system. At the present time, researches are being carried out considering a typical cell of the porous medium in order to investigate, in particular, this problem (Kaviany, 1995).

Darcy and Forchheimer terms are interpreted in this work as the momentum exchange between solid and fluid as follows (see, in general, Bowen, 1976, and in particular Deiber & Bortolozzi, 1998),

$$\mathbf{m}_f = -\mathbf{m}_s = -\frac{\mu_f^o}{K}\varepsilon^2 \mathbf{v}_f - \frac{b\rho_f^o}{K}\varepsilon^3 |\mathbf{v}_f|\mathbf{v}_f + p_f^o \nabla\varepsilon, \tag{17}$$

where the permeability $K(\varepsilon) = d_p^2\varepsilon^3/180(1-\varepsilon)^2$ and the empirical Forchheimer factor $b(\varepsilon) = 1.8d_p/180(1-\varepsilon)$ have been included (Prasad, Kulacki, & Keyhani, 1985; David, Lauriat, & Prasad, 1989).

Since porosity varies near the cavity walls (Benenati & Brosilow, 1962) an exponential decay of ε with the normal distance n is proposed as a first approximation,

$$\varepsilon = \varepsilon_\infty\left[1 + A\exp\left(-\frac{Bn}{d_p}\right)\right], \tag{18}$$

where A and B are empirical constants, and subscript ∞ indicates that porosity is evaluated far from walls. The values assigned to them in this work are 0.3 and 7.5, respectively. Following Vafai (1984), in Eq. (18) the exponential decay of porosity from the wall is taken into account by neglecting any spatial oscillations, which are considered to be a secondary effect.

Although a common practice is to use Eq. (18) to model approximately the porosity variation, a more rigorous description of this phenomenon involves an oscillatory damped porosity expressed (Martin, 1978; Mueller, 1991) as

$$\varepsilon = \varepsilon_{\min} + (1-\varepsilon_{\min})\xi^2, \quad -1 \leqslant \xi \leqslant 0 \tag{19}$$

and

$$\varepsilon = \varepsilon_\infty + (\varepsilon_{\min} - \varepsilon_\infty)\exp(-0.25\xi)\cos(3.51\xi), \quad \xi > 0, \tag{20}$$

where $\xi = 2(n/d_p) - 1$ and $\varepsilon_{\min} = 0.23$ is the minimum value of porosity.

Combining Eqs. (2) and (17), and including the constitutive equation for the stress tensor, the fluid momentum balance for the steady state is obtained. Additionally, the energy balances for fluid and solid phases result from Eqs. (3), (10), (11) and (14). In particular, the energy balance for the fluid is obtained from Eq. (3), where the internal energy is expressed $U_f = H_f - p_f/\rho_f$. Here, H_f is the enthalpy per unit of mass, and is a function of T_f and p_f. Therefore, the following model is obtained:

- *Continuity*:

$$\nabla\cdot(\rho_f^o \varepsilon \mathbf{v}_f) = 0. \tag{21}$$

- *Momentum balance of fluid*:

$$\rho_f^o \mathbf{v}_f\cdot\nabla\mathbf{v}_f = -\nabla p_f^o + \rho_f^o \mathbf{g} + \mu_f^o \nabla^2\mathbf{v}_f - \frac{\mu_f^o}{K}\varepsilon\mathbf{v}_f - \frac{b\rho_f^o|\mathbf{v}_f|}{K}\varepsilon^2\mathbf{v}_f. \tag{22}$$

- *Energy balance of fluid*:

$$\rho_f^o C_{pf}^o \varepsilon \mathbf{v}_f \cdot \nabla T_f = \nabla \cdot [(k_f \mathbf{I} + \mathbf{k}_d) \cdot \nabla T_f] - h_{sf} a_v (T_f - T_s) + \Phi + \beta T_f \varepsilon \mathbf{v}_f \cdot \nabla p_f^o. \quad (23)$$

- *Energy balance of solid*:

$$\nabla \cdot (k_s \nabla T_s) + h_{sf} a_v (T_f - T_s) = 0. \quad (24)$$

Eqs. (22) and (23) have been obtained by neglecting porosity gradients as suggested in the conclusions of our previous work (Deiber & Bortolozzi, 1998), which is also an assumption used and validated in most of the works considering this subject. In Eq. (23), $\Phi = -\boldsymbol{\tau}_f : \nabla \mathbf{v}_f$ is the viscous dissipation term, which can be neglected under the situation described below.

For a consistent interpretation of the numerical results reported in the discussion section, the two models (the 2-F above and the 1-F described below) are written in the following dimensionless variables: superficial velocity $\mathbf{V} = \varepsilon \mathbf{v}_f D/\alpha_{m\infty}$; fluid pressure $p^o = p_f^o K_\infty/\mu_f^o \alpha_{m\infty}$, where $\alpha_{m\infty} = k_{m\infty}/\rho_{fr}^o C_{pf}^o$; radial coordinate $R = r/D$ and axial coordinate $Z = z/D$. The fluid and solid dimensionless temperatures are $\Theta_f = (T_f - T_r)/\Delta T$ and $\Theta_s = (T_s - T_r)/\Delta T$, respectively. The characteristic scale for thermal conductivities is $k_{m\infty} = k_f^o \varepsilon_\infty + k_s^o (1 - \varepsilon_\infty) f_{c\infty}$. This procedure generates the Rayleigh, Darcy, Forchheimer and Prandtl numbers, respectively, as follows:

$$Ra = \frac{\rho_{fr}^o g \beta K_\infty D \Delta T}{\mu_f^o \alpha_{m\infty}}, \quad Da = \frac{K_\infty}{D^2},$$

$$Fs = \frac{b_\infty}{D}, \quad Pr_f = \frac{C_{pf}^o \mu_f^o}{k_f^o}.$$

An important relation useful for the discussion section is the fluid Rayleigh number $Ra_f = Ra/Da\lambda$ which involves fluid properties only. In this expression, $\lambda = k_f^o/k_{m\infty}$.

Additionally, the following dimensionless functions are generated:

$$\phi_0 = \frac{\rho_f^o}{\rho_{fr}^o}, \quad \phi_1 = \frac{K(\varepsilon)}{K_\infty}, \quad \phi_2 = \frac{b(\varepsilon)}{b_\infty},$$

$$\mathbf{k}_d^* = \frac{\mathbf{k}_d}{k_{m\infty}}, \quad H = \frac{6(1-\varepsilon)}{d_p} \frac{h_{sf} D^2}{k_{m\infty}}.$$

It is appropriate to point out here that in the procedure of writing the model in dimensionless form, the terms Φ and $\beta T_f \varepsilon \mathbf{v}_f \cdot \nabla p_f^o$ in Eq. (23) scale according to the following dimensionless numbers:

$$N_1 = \frac{2\mu_f^o k_{m\infty}}{\Delta T (\varepsilon_\infty \rho_{fr}^o C_{pf}^o D)^2}, \quad N_2 = \frac{\beta g D}{C_{pf}^o}.$$

Simple calculations indicate that these numbers are typically of the order of 10^{-15} and 10^{-7}, respectively, and hence, it is practical to neglect these terms in the model as far as the fluid has a viscosity of order of that of water (see also Section 7 and Deiber & Bortolozzi, 1998, for further details of the dimensional analysis presented above).

4. 1-F model for the porous medium

Case 1: *Local thermal equilibrium*

The 1-F model can be obtained from the 2-F model when $T_f = T_s = T$, which is the LTE assumption according to, for example, Amiri and Vafai (1994). Therefore, after summing equations (23) and (24) and neglecting the terms Φ and $\beta T_f \varepsilon \mathbf{v}_f \cdot \nabla p_f^o$ since N_1 and N_2 are very small, the energy balance is reduced to

$$\rho_f^o C_{pf}^o \varepsilon \mathbf{v}_f \cdot \nabla T = \nabla \cdot [(k_m \mathbf{I} + \mathbf{k}_d) \cdot \nabla T], \quad (25)$$

where $k_m = \varepsilon k_f^o + (1 - \varepsilon) k_s^o$ for the ideal mixture and $k_m = \varepsilon k_f^o + (1 - \varepsilon) k_s^o f_c$ when the Kunii and Smith's non-ideal expression for the stagnant thermal conductivity is used. Eq. (25) must be solved, of course, with Eqs. (21) and (22). It is also appropriate to mention here that Whitaker (1986) considered a temperature field T of the solid–fluid mixture before introducing the LTE assumption. In fact, this author analyzed in detail the constraints required to satisfy the LTE. This interesting theoretical aspect is also considered below, within the framework of the theory of mixtures for the non-local thermal equilibrium situation.

Case 2: *Non-local thermal equilibrium*

Although the LTE assumption can be used as a good approximation in many practical situations, it is recommended to carry out calculations with the 2-F model when T_f is substantially different from T_s. In these cases, the mixture properties are obtained from Eqs. (4) to (8) as described by the theory of mixtures. Therefore, one must evaluate ρ, $\mathbf{v}$, $\mathbf{T}$, $\mathbf{q}$ and U, which are the practical values required to characterize the mixture, from the 2-F model. Furthermore, it is clear that to obtain a 1-F model when the LTE assumption is not valid, an additional constraint that relates the values of T_f and T_s is required to achieve a closed mathematical problem (Whitaker, 1986). In this sense, one can also solve the 2-F model and then obtain the mixture properties.

Next, we present the framework to compare the predictions of the mixture properties calculated under the LTE assumption through the 1-F model — an approximation — with those obtained with the 2-F model and Eqs. (4) and (8) within the context of the theory of mixtures. This aspect is important to determine the LTE assumption should not be used as it is described in the physical conditions at which discussion section (see also Amiri & Vafai (1994) to visualize the importance of having criteria to establish these limits).

To proceed in this way, the Gibbs internal energy U of the mixture is assumed a function of temperature T and specific volume $\hat{v}$; thus $U = U(T,\hat{v})$, which is an appropriate constitutive expression for the mixture of water and rigid particles. Neglecting the small effects produced by changes of the specific volume on the evaluation of the internal energy ($N_2 \ll 1$), we consider $U \cong U(T)$ as a good approximation. This also indicates that the heat capacities at constant pressure and volume have similar values, for practical purposes. Therefore, the expression $\rho U = \rho C_{pm}(T - T_r)$ obtained with these considerations is combined with Eq. (8) to yield,

$$T = \frac{1}{\rho C_{pm}}\left(\rho_f C^o_{pf} T_f + \rho_s C^o_{ps} T_s + \frac{1}{2}\rho_f \mathbf{u}_f^2 + \frac{1}{2}\rho_s \mathbf{u}_s^2\right), \tag{26}$$

where

$$\rho C_{pm} = \rho^o_f \varepsilon C^o_{pf} + \rho^o_s (1-\varepsilon) C^o_{ps}. \tag{27}$$

Thus, the theory of mixtures gives a temperature T in Eq. (26) that is composed of two parts. One involves the solid and fluid temperatures averaged through the weighting factors $\rho_\alpha C^o_{p\alpha}/\rho C_{pm}$ for $\alpha = f, s$, while the other is associated to the phase drift velocities, the importance of which shall be determined numerically below.

5. Nusselt numbers

5.1. 2-F model

The momentum and energy balances, Eqs. (22)–(24) are solved using a finite-difference scheme, which is explained briefly in the next section. Once the flow and temperature fields are obtained numerically, the Nusselt numbers can be calculated as follows:

$$Nu_h = -\int_0^1 \left(\lambda\varepsilon \frac{\partial \Theta_f}{\partial R} + \nu(1-\varepsilon) f_c \frac{\partial \Theta_s}{\partial R}\right) \mathrm{d}Z \quad \text{at } R = \frac{r_i}{D} \tag{28}$$

and

$$Nu_c = -\int_0^1 \left(\lambda\varepsilon \frac{\partial \Theta_f}{\partial R} + \nu(1-\varepsilon) f_c \frac{\partial \Theta_s}{\partial R}\right) \mathrm{d}Z \quad \text{at } R = \frac{r_o}{D}, \tag{29}$$

which are evaluated at the hot and cold walls, respectively. In these equations $\nu = k^o_s/k_{m\infty}$.

The dimensionless numbers Nu_h and Nu_c must satisfy the relation

$$Nu_h = \kappa Nu_c, \tag{30}$$

where $\kappa = r_o/r_i$ is the radius ratio (see also Prasad & Kulacki, 1984). Eq. (30) indicates that the heat entering the cavity through the hot wall has to be equal to the heat leaving the cavity at the cold wall for steady heat transfer.

We carried out, in addition, a more rigorous cross-checking of numerical results through a macroscopic balance of energy in a volume fraction of the porous cavity comprised between the hot wall and any vertical cut placed at a radius between r_i and r_o. Thus, placing the cavity cut at $(r_i + r_o)/2$, numerical results shall satisfy, in addition to Eq. (28), the following expression:

$$Nu_h = \frac{(\kappa+1)}{2}\int_0^1 \left[-(\lambda\varepsilon + k^*_d)\frac{\partial \Theta_f}{\partial R} - \nu(1-\varepsilon) f_c \frac{\partial \Theta_s}{\partial R} + V_r \Theta_f \right] \mathrm{d}Z, \tag{31}$$

where V_r is the radial component of velocity $\mathbf{V}$ and $k^*_d = \gamma l(n) a|\mathbf{V}|$ (see Eqs. (12) and (13)) is the isotropic dispersive thermal conductivity in dimensionless form. In Eq. (31), the integral term represents the Nusselt number evaluated at $R = (r_i + r_o)/2D$; this value multiplied by $(\kappa + 1)/2$ gives the Nusselt number at the hot wall.

5.2. 1-F model

When the 1-F model with the LTE assumption is solved, the temperature field obtained allows us to evaluate the Nusselt number in both vertical walls. In fact, for this case Eqs. (28) and (29) reduce to,

$$Nu_h = -\int_0^1 k^*_m \frac{\partial \Theta}{\partial R} \mathrm{d}Z \quad \text{at } R = \frac{r_i}{D} \tag{32}$$

and

$$Nu_c = -\int_0^1 k^*_m \frac{\partial \Theta}{\partial R} \mathrm{d}Z \quad \text{at } R = \frac{r_o}{D}, \tag{33}$$

where $k^*_m = k_m/k_{m\infty}$ and $\Theta = (T - T_r)/\Delta T$, so that $T = T_f = T_s$.

A similar result to that expressed by Eq. (31) can be also obtained for the 1-F model as follows:

$$Nu_h = \frac{(\kappa+1)}{2}\int_0^1 \left[-(k^*_m + k^*_d)\frac{\partial \Theta}{\partial R} + V_r \Theta \right] \mathrm{d}Z, \tag{34}$$

where the integral term is the Nusselt number evaluated at $R = (r_i + r_o)/2D$.

From Eqs. (31) and (34), it is clear that the Nusselt numbers for the 2- and 1-F models present different terms associated to conduction and convection of heat in the cylindrical surface placed, for example, at $(r_i + r_o)/2$ when the LTE assumption is not valid. In this particular situation, the velocity profile V_r of the 2-F model is

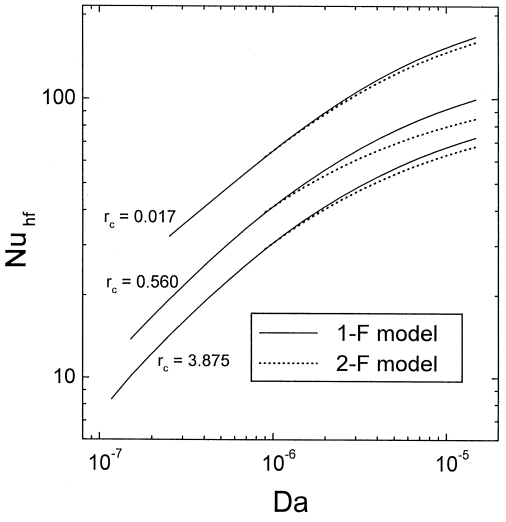

Fig. 2. Fluid Nusselt number Nu_{hf} obtained from 1- and 2-F models as function of Darcy number for different values of the conductivity ratio r_c and $Ra_f = 2.1 \times 10^9$. Other parameters are: $Pr_f = 4.60$, $L/D = 1$, $\varepsilon_\infty = 0.40$, $A = 0.35$, $B = 7.5$, $a_l = a_t = 0.1$, $\omega = 2.5$.

different from that of the 1-F model (see also Fig. 5). Thus, the value of Nu_h obtained from Eq. (31) cannot be equal to Eq. (34) unless the LTE is satisfied.

Before ending this section, it is useful to define the fluid Nusselt number at the hot wall Nu_{hf} in terms of the Nusselt number Nu_h (see Eqs. (28) and (32)) to account properly the effect of a variable r_c. Thus, $Nu_{hf} = Nu_h/\lambda$.

6. Numerical method

Eqs. (21) and (22) used in both the 2- and 1-F models are rewritten using the vorticity-stream function scheme. The resulting models (Eqs. (21)–(24) for the 2-F model and Eqs. (21), (22) and (25) for the 1-F model) are expressed in finite differences as follows: (1) Convective terms are discretized with the second upwind technique (Roache, 1972). (2) Central differences are used for second derivatives. (3) Heat conduction terms with variable effective conductivities on the right-hand side of Eqs. (23) and (25) are discretized according to the procedure described by Peaceman (1977). The discrete equations are solved using the relaxation method through successive iterations as it was described in the work of Peirotti, Giavedoni, and Deiber (1987). The iteration procedure is continued until a convergence criterion is satisfied as follows:

$$\frac{\sum_{ij} |s_{ij}^{k+1} - s_{ij}^{k}|}{\sum_{ij} |s_{ij}^{k}|} \leqslant \sigma, \tag{35}$$

where s_{ij} is the dependent variable that is being numerically calculated (vorticity, stream function and temperatures of fluid and solid). The subscripts i and j imply spatial position in the computational mesh, and k refers to the iteration number. In this work, the value assigned to σ is 10^{-6}.

Since high values of Ra generate thermal and momentum boundary layers near the cavity walls, it is highly recommended to carry out a coordinate transformation so that grid intervals are very small (of the order of 10^{-3}) near these walls. In this work, the coordinate transformation proposed by Kálnay de Rivas (1972) is used (for details, see Deiber & Bortolozzi, 1998). On the other hand, this transformation yields a coarse mesh at the cavity center. This interplay between mesh sizes and cavity zones requires a careful verification of consistency between numerical evaluations and macroscopic energy balance. Therefore, in order to control the consistency of computational calculations, a numerical parameter is defined as follows:

$$\chi = \frac{Nu_h}{\kappa Nu_c}. \tag{36}$$

Thus, the numerical procedure is giving consistent results when $\chi \to 1$. This requirement is a severe test for the accuracy of results, and this limit is only attained with an appropriate combination of small grid intervals and rather small values of σ.

7. Results and discussion

This section presents our results from two points of view. One includes most of the calculations considering the variable porosity given by Eq. (18), which is a good approximation for applications. The second one analyzes numerical results with Eqs. (19) and (20) to elucidate how the spatially damped oscillations of porosity (validated experimentally in the literature) affect both the Nusselt number and the flow field predicted with these models.

Thus, first numerical studies were carried out with Eq. (18) to compare the 2- and the 1-F models, the second one being formulated with the LTE assumption. Results demonstrate that the Nusselt numbers and the velocity profiles predicted from these two models are not the same, when $T_f \neq T_s$ in the porous matrix, in the context of the 2-F model. The opposite is also true when the LTE assumption is attained and physically approximated in the whole bed. Therefore, to visualize better these physical aspects under analysis, the LTE situation shall be violated by changing the Darcy number and the conductivity ratio. We discuss these effects separately below.

To quantify the influence of the Darcy number while the other dimensionless numbers are kept constant, the particle diameter has to be changed. This also implies that the other parameters like particle material, interstitial fluid, temperature difference between hot and cold

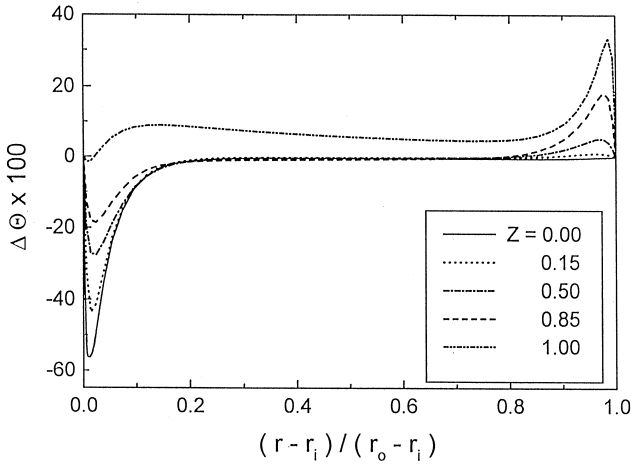

Fig. 3. Percentile difference between fluid and solid dimensionless temperatures $\Delta\Theta \times 100$ as function of radial position $(r - r_i)/(r_o - r_i)$ for different heights z of the porous cavity. Parameters are: $Ra_f = 2.1 \times 10^9$, $Da = 0.99 \times 10^{-5}$, $Pr_f = 4.60$, $L/D = 1$, $r_c = 0.56$, $\varepsilon_\infty = 0.40$, $A = 0.35$, $B = 7.5$, $\gamma = 0.10$, $a_l = a_t = 0.1$, $\omega = 2.5$.

walls and cell dimensions have also to be fixed for these particular numerical runs. One thus gets a change of the bed permeability, and hence, of the Darcy number. We found that increasing Da, while r_c was constant, the fluid Nusselt numbers calculated from the 1- and 2-F models also increased. Additionally, the values of Nu_{hf} obtained from these models are not the same, as shown in Fig. 2. In fact, for the water–glass system ($r_c = 0.56$) and $Da = 1.1 \times 10^{-6}$, the difference between the values of Nu_{hf} (Eqs. (28) and (32)) is less than 1%, while for $Da = 0.99 \times 10^{-5}$ is around 15.4%. In all the cases studied here, the two models provide almost the same Nusselt numbers for $Da < 10^{-6}$; i.e. the 1-F model is good to predict quantitatively this macroscopic parameter at relatively low Darcy numbers. On the other hand, when porous media of high permeability are considered (high Da), numerical results indicate that the 1-F model overestimates the steady heat flux through the porous cavity, for any value of r_c considered in Fig. 2. The reason for this defect to occur (Deiber & Bortolozzi (1998) fitted experimental data with the 2-F model and physicochemical properties used here) is that the 1-F model does not take into account the additional resistance $1/h_{sf}$ (Eq. (15)) to the interfacial heat transfer that exists in the microstructure of the cavity between the solid particles and the fluid. This result is emphasized when the particle diameter is relatively large, because the heat transfer becomes difficult to occur when the specific surface a_v of the porous medium is low. It is important to place emphasis in that the two models predict near the same Nu_{hf} when the local heat transfer between the interstitial fluid and the particles is high, yielding equal or almost equal temperatures in both phases. This last situation occurs mainly for porous media with small particles, i.e., for $\gamma \to 0$ (see also Bortolozzi & Deiber, 1998).

We also analyzed the effect of the thermal conductivity ratio $r_c = k_f^o/k_s^o$ on the fluid Nusselt number Nu_{hf}. With this purpose, numerical runs were carried out by keeping k_f^o constant and taking different values of k_s^o. In practice, these situations are obtained by changing the material of which the spheres are made. For this purpose the same fluid was used and ΔT was kept constant in all the cases so that Ra_f and Da remained constant too. These considerations allowed us to study specifically the effect of r_c on Nu_{hf}. Therefore, the thermophysical properties of three systems were used: water–steel, water–glass and water–acrylic (Nield, 1991; Prasad et al., 1989; these references report experimental values of stagnant thermal conductivities of the porous media considered here). It is found that for high Darcy numbers, the physical situation is close to that of the LTE in the porous medium when the solid phase is a good heat conductor ($r_c \to 0$). This result is expected because the high thermal conductivity of the solid improves the heat transfer between the interstitial fluid and the particles. For this particular reason, i.e. when the system is close to the LTE, the Nusselt numbers calculated with both models are similar in the whole range of values of Da. For example, in Fig. 2, the difference between the Nusselt numbers is no more than 2.8% for $Da = 0.99 \times 10^{-5}$ and $r_c = 0.017$.

On the other hand, when the solid phase is a poor heat conductor and the bed permeability is relatively high, numerical results show that differences between solid and fluid temperatures in some places of the porous medium are present. Thus, for $r_c = 0.56$ (water–glass system) and $Da = 0.99 \times 10^{-5}$, zones in the cavity with dimensionless percentile temperature differences $\Delta\Theta \times 100$ between phases ranging from -55.1 to $+32.5\%$ are found. For a less heat conductor solid phase like acrylic spheres saturated with water ($r_c = 3.875$), these differences are -63.3 and $+38.9\%$, respectively. Nevertheless, this effect is not directly related with the numerical Nusselt numbers obtained from the two models, as shown clearly in Fig. 2, in particular for $r_c = 3.875$. In fact, the higher differences between Nusselt numbers occurs for intermediate values of r_c. When $r_c = 0.56$ and $Da = 0.99 \times 10^{-5}$, this difference is around 15.4%, while for $r_c = 3.875$ and $Da = 0.99 \times 10^{-5}$, it is smaller and around 6.5%. Consequently, these numerical results show one that despite the Nusselt numbers may be close from one another as calculated from the 1- and 2-F models, respectively, it is also possible to find for these calculations, zones in the porous cavity where the differences between phase temperatures are significant for high r_c. Then, the comparison between Nusselt numbers (which are macroscopic parameters) obtained with these models cannot indicate us, in a sufficient way, that the LTE assumption is attained at the microscopic level under certain physical conditions. It may happen that even in the case of existing high differences between solid and fluid temperatures in some places of the cavity, there are physical reasons for

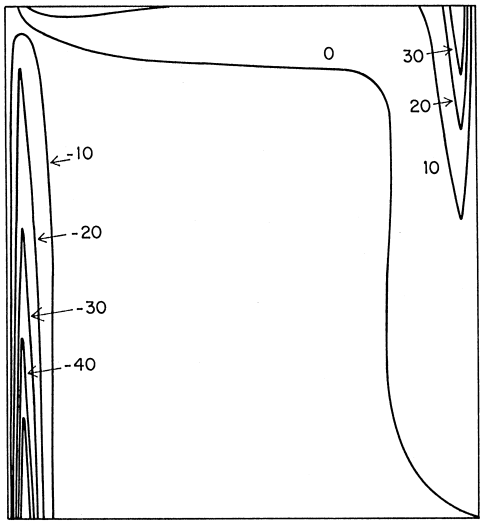

Fig. 4. Map of percentile difference between fluid and solid dimensionless temperatures $\Delta\Theta \times 100$ in the porous cavity. Parameters are the same as in Fig. 3.

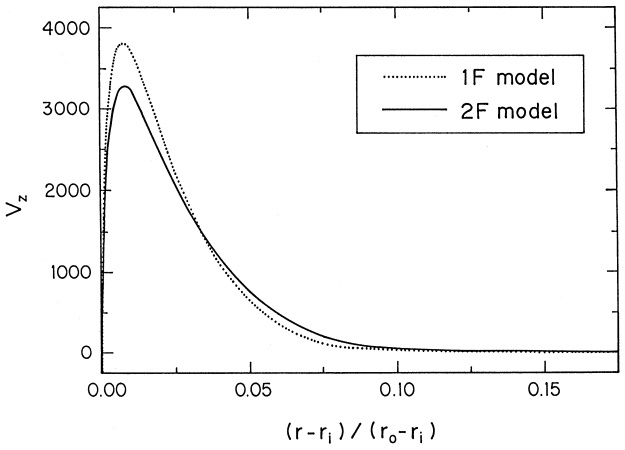

Fig. 5. Dimensionless velocity V_z near the hot wall at midheight of the porous cavity, obtained from 1- and 2-F models, as function of radial position $(r - r_i)/(r_o - r_i)$. Parameters are the same as in Fig. 3.

yielding similar Nusselt numbers from these models. In this sense a physical interpretation for high r_c follows. Thus, when k_s^o is substantially smaller than k_f^o, the contribution of the solid phase to the global heat transfer through vertical walls is poor. This result can be visualized from Eqs. (28) and (32). In fact, under this situation, $Nu_h \approx -\int_0^1 \lambda\varepsilon(\partial\Theta_f/\partial R)\,\mathrm{d}Z$ for the 2-F model. A similar expression is obtained for the 1-F model since k_m^* is close to $\lambda\varepsilon$ for $v \ll \lambda$. Therefore, when $k_s^o \ll k_f^o$, Eqs. (28) and (32) give almost the same Nusselt number at the hot wall, despite the solid temperature is different from the fluid temperature in some places of the porous medium.

We found that the greatest differences between the temperatures of solid and fluid phases are in zones close to the vertical walls of the cavity. Additionally, under the circumstances analyzed in this work, the solid temperature T_s is greater than the fluid temperature T_f near the hot wall. This specific relation is the opposite in the neighborhood of the cold wall. The temperature differences obtained near the hot wall are higher than those calculated near the cold wall due to the annular geometry of the cavity (the surface of heating is smaller than the surface of cooling). On the other hand, the middle zone of the cavity is close to the LTE conditions as it is required in the 1-F model. These results can be readily visualized in Fig. 3 for different cuts along the cavity height. The maximum difference in absolute value between fluid and solid dimensionless temperatures $|\Delta\Theta|$ is thus placed on the bottom near the hot wall of the cavity. These thermal responses are consistent with the expected behavior followed by the convective streams of the cold fluid, which approaches the hot wall from below. Then, this fluid gets hotter when it moves upward, and its temperature becomes closer to that of the solid phase. At the isolated top wall ($Z = 1$) the temperatures of the phases do not become equal and T_f is higher than T_s; this result is satisfied along the whole width of the cavity. Thus, the fluid that flows in the upper boundary layer does not deliver enough heat to the solid particles and both phases cannot be at LTE near the upper isolated wall, in this particular cavity where $L = D$.

Fig. 4 presents a map showing the iso-lines of $\Delta\Theta$ as they are predicted by the 2-F model for the more drastic situation analyzed here, i.e. when the Darcy number and the conductivity ratio are relatively high. The iso-line corresponding to $\Delta\Theta = 0$ divides the cavity in two zones. Each zone has the thermal characteristics mentioned above. This figure also shows where the near LTE domain is placed in the cavity as well as the zones where $\Theta_f < \Theta_s$ (low and left cavity zone) and $\Theta_f > \Theta_s$ (upper and right cavity zone). Thus, the two maxima of $|\Delta\Theta|$ are diagonally opposed in the cavity.

To determine quantitatively the limit of application of the LTE assumption according to the criteria similar to those established by Amiri and Vafai (1994), we calculated the fractions of the cell volume where temperature differences satisfy the following prefixed ranges: (1) $0 \leqslant |\Delta\Theta| \times 100 \leqslant 1$; (2) $1 < |\Delta\Theta| \times 100 \leqslant 5$; (3) $5 \leqslant |\Delta\Theta| \times 100 \leqslant 10$; (4) $10 < |\Delta\Theta| \times 100 \leqslant 20$ and (5) $20 < |\Delta\Theta| \times 100$. Table 1 presents the results obtained for $Ra_f = 2.1 \times 10^9$ and different Darcy numbers. It is found that for beds of low permeability ($Da = 1.7 \times 10^{-7}$) a significant volume fraction of the cavity has percentile temperature differences less than 1%, indicating this result that the LTE assumption is good except for some zones that surmount only around 7% of the total volume of the cavity. In fact, for $Da = 1.1 \times 10^{-6}$, around 37% of the cavity volume presents values of $|\Delta\Theta| \times 100$ comprised

Table 1
Percentile of cavity volume that presents temperature differences within prefixed ranges, for different values of Da and $Ra_f = 2.1 \times 10^9$. The other parameters are the same as in Fig. 3

$\lvert\Delta\Theta\rvert \times 100$	0–1	1–5	5–10	10–20	> 20
$Da = 1.7 \times 10^{-7}$	93	7	0	0	0
$Da = 1.1 \times 10^{-6}$	63	35.5	1.5	0	0
$Da = 0.99 \times 10^{-5}$	24	49	12.5	9	5.5

Table 2
Percentile of cavity volume that presents temperature differences within prefixed ranges, for different values of Ra_f and $Da = 0.99 \times 10^{-5}$. The other parameters are the same as in Table 1

$\lvert\Delta\Theta\rvert \times 100$	0–1	1–5	5–10	10–20	> 20
$Ra_f = 2.0 \times 10^7$	79	21	0	0	0
$Ra_f = 1.8 \times 10^8$	57	38	5	0	0
$Ra_f = 2.1 \times 10^9$	24	49	12.5	9	5.5

Table 3
Maximum percentile differences between fluid and solid dimensionless temperatures $\Delta\Theta \times 100$ obtained with different correlations for h_f (see Eq. (16)). r_c refers to the conductivity ratio of the three systems studied

	$r_c = 3.875$	$r_c = 0.56$	$r_c = 0.017$
Correlation (a)	− 63.27 38.89	− 55.10 32.45	− 57.62 29.54
Correlation (b)	− 64.24 39.54	− 61.24 35.98	− 64.68 33.09
Correlation (c)	− 63.20 38.80	− 54.72 31.90	− 57.37 28.81

Table 4
Fluid Nusselt numbers Nu_{hf} obtained with different correlations for h_f (see Eq. (16)). r_c refers to the conductivity ratio of the three systems studied

	$r_c = 3.875$	$r_c = 0.56$	$r_c = 0.017$
Correlation (a)	65.99	82.86	146.72
Correlation (b)	65.91	80.53	131.23
Correlation (c)	66.00	82.90	147.16

between 1 and 10%. For $Da = 0.99 \times 10^{-5}$ (high permeability bed) more than 60% of the cavity presents values within the range 1–10% and there exist zones with percentile differences higher than 20%, indicating these results that the description of the porous medium through the 1-F model is an approximation. This discussion validates our previous conclusion described above: the volumetric fraction with unequal temperatures of solid and fluid phases increases with the Darcy number. Table 2 shows the results for high permeability beds ($Da \cong 10^{-5}$) at different Ra_f. Additionally, an increase of the fluid Rayleigh number, keeping Da constant, generates small zones with very high $\lvert\Delta\Theta\rvert \times 100$ in this porous medium of high permeability.

Although the results shown in Fig. 4 were obtained with the correlation of Wakao et al. (1979), additional calculations were also carried out by using Correlations (b) and (c) also described by Eq. (16) where numerical coefficients are different from those of Correlation (a). It is observed that these three correlations, which have a value of h_f different from zero when $Re_p \to 0$, give almost the same numerical results, in the sense that relatively small changes in the maximum temperature differences and Nusselt numbers are observed (see Tables 3 and 4). Thus, the description of particular situations showing $\Delta\Theta \neq 0$ does not depend significantly on the type of correlation used to evaluate the interface heat transfer coefficient.

In the context of this work, it is also important to point out that the heat transfer between phases increases with Ra_f, mainly due to fluid convection through the interstices of the porous matrix. Nevertheless, in beds of higher particle diameters (low a_v) this last effect is not sufficient to generate equal temperatures at every points of the porous medium. This phenomenon occurs because the solid resistance to the local heat flux is limiting, and hence, controlling the heat transfer process (see Eq. (15)). Thus, in this case the increase of h_f does not necessarily produce an important effect on the global heat transfer between the fluid and solid particles.

It is also remarkable that the velocity fields obtained from the 1- and 2-F models are not coincident, unless the LTE is physically approximated (see Fig. 5). This is partly due to the way the thermal driving force associated to the gravity term is calculated in the 1-F model. In this model, this force is the difference between the fluid temperature taken equal to the solid temperature, and the reference temperature T_r that is the arithmetic mean between T_h and T_c. On the other hand, in the 2-F model the fluid movement near the particle is driven by a difference between the fluid temperature T_f, which is not necessarily equal to the solid temperature T_s, and reference temperature. At low Rayleigh and Darcy numbers, these velocity profiles are rather coincident, because $T_s \approx T_f$.

According to our results, the fluid phase shows temperature profiles that are sharper than those of the solid phase, close to the vertical cavity walls. As we mentioned above, the single temperature profile calculated with the 1-F model considering the LTE, generates a driving force in the gravity term that is different from that of the 2-F model for the cases studied here. Additionally, the differences in velocity fields obtained from the two models also affect the value of the Nusselt number as it can be visualized from Eqs. (31) and (34), where the presence of

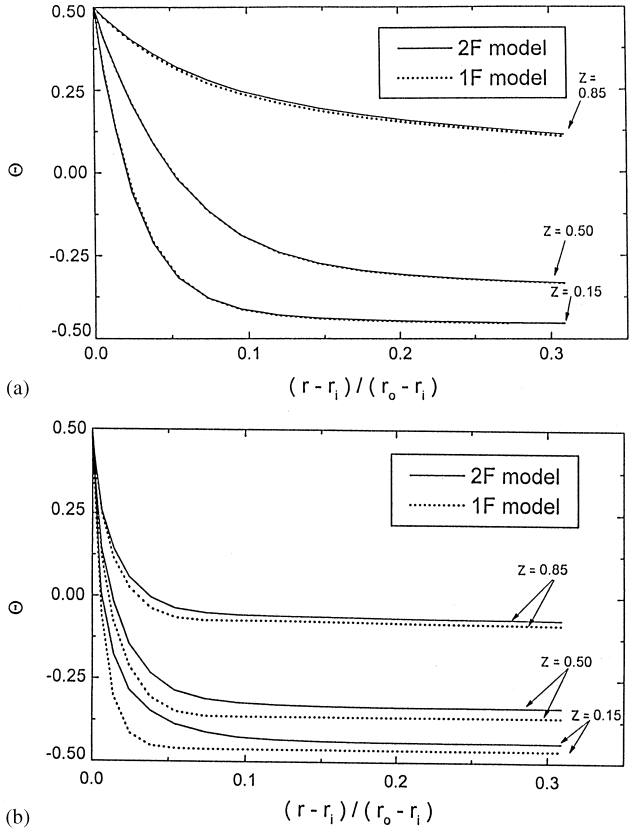

Fig. 6. Dimensionless mixture temperature Θ obtained from 2- and 1-F models for $Ra_f = 2.1 \times 10^9$, $r_c = 0.56$ and different values of Darcy number. (a) $Da = 1.7 \times 10^{-7}$, (b) $Da = 0.99 \times 10^{-5}$. The other parameters are the same as in Fig. 2.

the velocity component V_r is evident. In this context of analysis, it is clear that the 2-F model predicts Nusselt numbers that are not equal to those calculated with the 1-F model because both the temperature and velocity profiles of each model are different, unless the LTE assumption is attained in the porous cavity.

Another analysis that illustrates comparative aspects between these models consists in calculating the mixture temperature by means of Eq. (26). This calculation requires the knowledge of both the temperatures and drift velocities of the solid and fluid phases, which are a result of solving the 2-F model only (Eqs. (21)–(24)). For different Darcy numbers, the mixture temperature profiles thus calculated are compared with the temperature profiles obtained with the 1-F model involving the LTE assumption (Fig. 6). In this figure, one can observe that the temperature profiles calculated with the two models are almost coincident when the bed is composed of particles with small diameters ($Da = 1.7 \times 10^{-7}$) (Fig. 6(a)). The opposite occurs for beds with high particle diameters ($Da = 0.99 \times 10^{-5}$), particularly in the zone near the hot wall (Fig. 6(b)). This conclusion is consistent with the fact that at high Da the 1-F model overestimates the Nusselt number in relation to the experimental values available for this problem for the set of data used in the 2-F model.

Additionally, we found numerically that in Eq. (26) (see also Eq. (8)) the terms associated to the drift velocities of the fluid and solid phases can be neglected as a good approximation. This result is further verified when one evaluates the order of magnitude of the terms involving these velocities, which are around 10^{-9} in the dimensionless model. In a similar analysis, numerical results also reveal that the terms involving drift velocities are negligible in Eq. (7), except $\rho_\alpha U_\alpha \mathbf{u}_\alpha$ containing U_α, which is a part of the energy convective term, when the energy balance is expressed by using the mixture velocity v.

As far as water is the fluid phase in the porous media considered in this work, the dissipation term can be always neglected in the energy balance for both models. Thus, for the porous cavity studied here, with for example $\Delta T = 20^\circ$C, and the water thermophysical properties evaluated at 40°C, the values of the dimensionless parameter N_1 and N_2 are of the order of 10^{-15} and 10^{-7}, respectively. When one includes the terms associated to N_1 and N_2 in the numerical algorithm, no relevant differences are observed from the numerical values obtained by neglecting these terms.

Finally, numerical studies were carried out with Eqs. (19) and (20) included into the 2- and the 1-F models. Results demonstrate here that the Nusselt numbers are not significantly affected when a damped oscillating porosity is considered in these models. Although both porosity functions (Eqs. (18)–(20)) yield similar values of Nusselt numbers for practical use, this conclusion is not valid when the flow field is under analysis. In fact, Fig. 7 shows that 2- and 1-F models predict spatially oscillating streamlines following the periodic change in porosity when Eqs. (19) and (20) are applied. Since the permeability of the cavity is a function of the porosity one expects this phenomenon to be present. Therefore, it is clear that Eqs. (19) and (20) should be used in 1- and 2-F models when fluid convection at the microstructure level is relevant, for instance, in industrial devices where mass transfer with chemical reaction takes place within a bed of particles of relatively high permeability.

8. Conclusions

The Nusselt number evaluated through the 2-F model is less or equal to the value obtained from the 1-F model under the LTE assumption, for the same set of parameters and thermophysical properties, because the 1-F model does not include the additional resistance to the heat transfer existing in the microstructure of the cavity between the solid particles and the interstitial fluid. Numerical results indicate that the 1-F model should be used for porous media in which the Darcy number is less than 10^{-5} in the porous cavity studied.

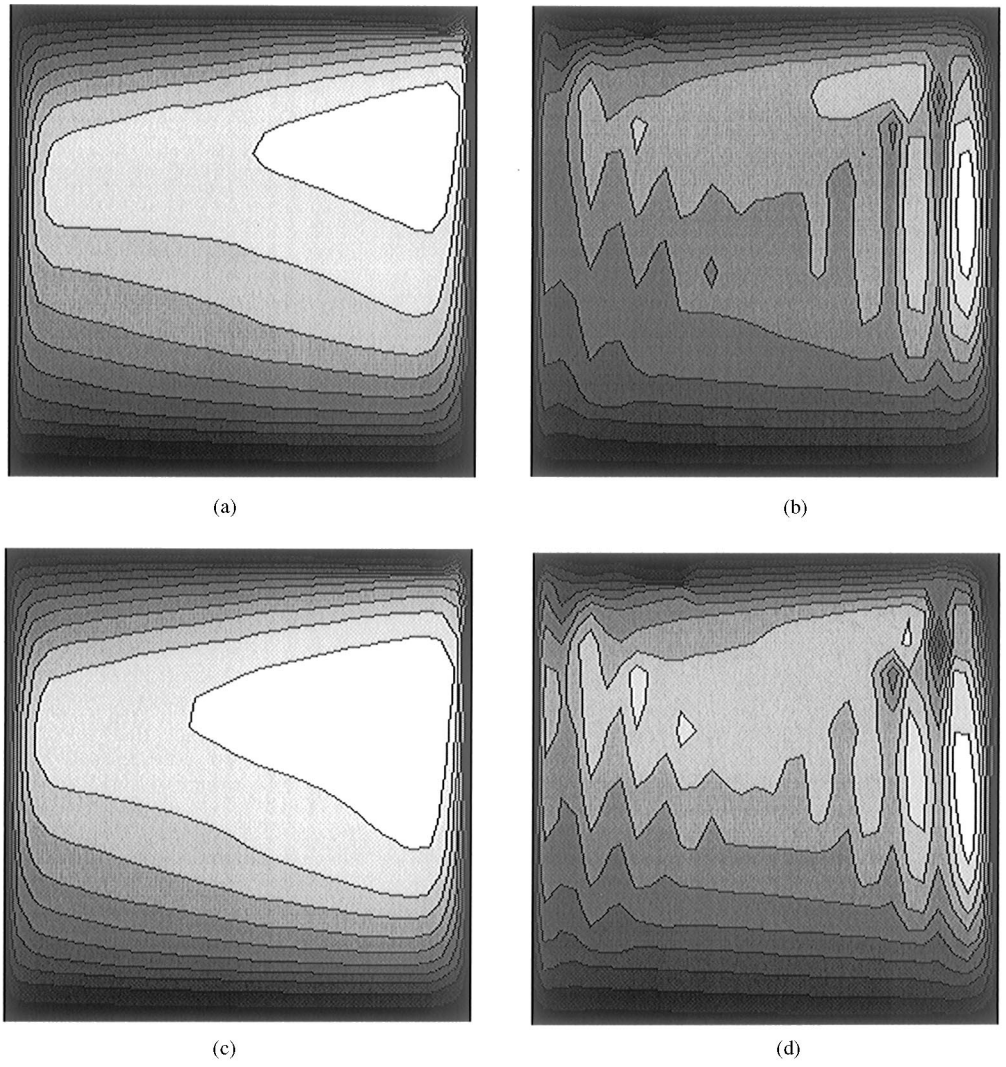

Fig. 7. Numerical predictions of flow patterns in the porous cavity. Hot vertical wall is on the left. Parameters are the same as in Fig. 3. Ten equally spaced streamlines are reported between the maximum value Ψ_{max} and the minimum $\Psi_{min} = 0$. (a) 1-F model with Eq. (18); $\Psi_{max} = 34.53$. (b) 1-F model with Eqs. (19) and (20); $\Psi_{max} = 38.03$. (c) 2-F model with Eq. (18); $\Psi_{max} = 30.45$. (d) 2-F model with Eqs. (19) and (20); $\Psi_{max} = 32.98$.

Although the LTE assumption can be used as a good approximation in many practical situations, it is recommended to carry out calculations with the 2-F model when the solid temperature is substantially different from the interstitial fluid temperature. On the other hand, the formulation of a 1-F model when the LTE assumption is not attained requires an additional constraint that relates T_f with T_s to get a closed mathematical problem. This constraint is not available, unless one proposes empirical relationships or generates an additional modeling. One possible solution to this problem is the 2-F model.

For a porous medium of high permeability composed by fluid and solid particles of low thermal conductivity, zones of the bed with differences between temperatures exist. The comparison between Nusselt numbers predicted through the 1- and 2-F models cannot indicate us precisely when the LTE assumption is attained at the microscopic level.

Another important aspect to be considered in the modeling of the heat transfer by natural convection in porous media is the formulation of the thermal driving force associated to the gravity term. Finally, if the fluid convection is required at the microstructure level, a damped oscillating porosity function shall be used in 1- and 2-F models.

Notation

a	thermal hydrodynamic dispersivity tensor
a_l	longitudinal component of the dispersivity tensor
a_t	transverse component of the dispersivity tensor
a_v	specific surface of the porous medium, m^{-1}

a_1 empirical constant for Kunii and Smith's correlation
A empirical constant used in Eq. (18)
b Forchheimer inertial constant, m
B empirical constant used in Eq. (18)
c numerical constant used in Eq. (16)
C^o_{pf} fluid heat capacity at constant pressure, J/kg K
C_{pm} heat capacity of fluid–solid mixture, J/kg K
d_p particle diameter, m
D width of the porous cavity, m
Da Darcy number ($= K_\infty/D^2$)
e_α exchange of internal energy, W/m^3 ($\alpha = s,f$)
e^T_α exchange of total energy, W/m^3 ($\alpha = s,f$)
f_c factor for Kunii and Smith's correlation
F_s Forchheimer number ($= b_\infty/D$)
$\mathbf{g}$ acceleration due to gravity, m/s^2
h_f fluid heat-transfer coefficient, W/m^2 K
h_{sf} solid–fluid heat-transfer coefficient, W/m^2 K
H dimensionless heat-transfer coefficient
H_f fluid enthalpy, J/kg
$\mathbf{I}$ unity tensor
k_α thermal conductivity of species in mixture, W/m K ($\alpha = s,f$)
k_m thermal conductivity of the saturated porous medium, W/m K
k^*_m ($= k_m/k_{m\infty}$)
$\mathbf{k}_d$ thermal dispersion tensor, W/m K
$\mathbf{k}^*_d$ ($= \mathbf{k}_d/k_{m\infty}$)
K permeability of the porous medium, m^2
l van Driest function
l_c characteristic length for heat transfer in the solid phase, m
L height of the porous cavity, m
m numerical constant used in Eq. (16)
$\mathbf{m}_\alpha$ exchange of momentum, Pa/m ($\alpha = s,f$)
n perpendicular distance from any wall, m
Nu_i overall Nusselt numbers defined in Eqs. (28)–(34) ($i = h,c$)
$Nu_{h,f}$ overall Nusselt number at hot wall, based upon fluid conductivity
p^o_f fluid pressure, Pa
p dimensionless fluid pressure
P_{rf} fluid Prandtl number ($= C^o_{pf}\mu^o_f/k^o_f$)
q numerical constant used in Eq. (16)
$\mathbf{q}$ heat flux of mixture, W/m^2
$\mathbf{q}_\alpha$ heat flux of species, W/m^2 ($\alpha = s,f$)
r radial coordinate, m
r_c conductivity ratio ($= k^o_f t/k^o_s$)
r_i inner radius of porous cavity, m
r_o outer radius of porous cavity, m
R ($= r/D$)
Ra Rayleigh number ($= \rho^o_{fr} g\beta K_\infty D\,\Delta T/\mu^o_f \alpha^o_{m\infty}$)
Ra_f fluid Rayleigh number ($= Ra/Da\lambda$)
Re_p particle Reynolds number ($= \rho^o_{fr}\,\varepsilon|\mathbf{v}_f|d_p/\mu^o_f$)
s numerical constant used in Eq. (16)
t time, s
$\mathbf{T}$ stress tensor of mixture, Pa
T temperature of mixture, K
T_α species temperature, K ($\alpha = s,f$)
T_i wall temperature, K ($i = h,c$)
$\mathbf{T}_f$ fluid stress tensor, Pa
T_r reference temperature, K
$\mathbf{u}_\alpha$ diffusion velocity of species, m/s ($\alpha = s,f$)
U internal energy of mixture, J/kg
U_α internal energy of species, J/kg ($\alpha = s,f$)
$\hat{v}$ specific volume, m^3/kg
$\mathbf{v}$ velocity of mixture, m/s
$\mathbf{v}_f$ fluid velocity, m/s
$\mathbf{V}$ dimensionless superficial velocity
V_j component of dimensionless superficial velocity ($j = r,z$)
z axial coordinate, m
Z ($= z/D$)

Greek letters

α^o_m thermal diffusivity of saturated porous medium, m^2/s
β isobaric thermal expansion coefficient, K^{-1}
γ ($= d_p/D$)
ε porosity
Θ_f [$= (T_f - T_r)/(T_h - T_c)$]
Θ_s [$= (T_s - T_r)/(T_h - T_c)$]
κ ($= r_o/r_i$)
λ ($= k^o_f/k_{m\infty}$)
μ^o_f fluid viscosity, Pa s
ν ($= k^o_s/k_{m\infty}$)
ξ [$= 2(n/d_p) - 1$]
ρ density of mixture, kg/m^3
ρ_α species density in mixture, kg/m^3 ($\alpha = s,f$)
φ_j empirical constants for Kunii and Smith's correlation ($j = 1,2$)
ϕ_j functions used in the dimensionless model ($j = 0$–2)
Φ viscous dissipation term, W/m^3
σ numerical average error defined by Eq. (35)
$\boldsymbol{\tau}_f$ viscous stress tensor of fluid, Pa
χ numerical parameter defined by Eq. (36)
ψ [$= 1 + 1.5(1 - \varepsilon)$]
Ψ streamlines
ω van Driest empirical constant

Subscripts

c cold wall
f fluid phase
h hot wall
m property of composite (solid and fluid)
min minimum value
max maximum value
r reference temperature
s solid phase
∞ any property far from cavity walls

Superscripts

o	property of pure species
t	total property

Acknowledgements

The authors wish to thank the financial aid received from CONICET (Consejo Nacional de Investigaciones Científicas y Técnicas de Argentina) and from Secretaría de Ciencia y Técnica de la UNL (Universidad Nacional del Litoral, Argentina) — Programaciones CAI + D 94 y 96.

References

Amiri, A., & Vafai, K. (1994). Analysis of dispersion effects and non-thermal equilibrium, non-Darcian, variable porosity incompressible flow through porous media. *International Journal of Heat and Mass Transfer*, *6*, 939–954.

Benenati, R. F., & Brosilow, C. B. (1962). Void fraction distribution in beds of spheres. *A.I.Ch.E. Journal*, *8*(3), 359–361.

Bird, R. B., Stewart, W. E., & Lightfoot, E. N. (1960). *Transport phenomena*. New York: Wiley (Chapters 6 and 13).

Bortolozzi, R. A., & Deiber, J. A. (1998). Two- and one-field models for natural convection in porous media. *Latin American Applied Research*, *28*(1/2), 69–74.

Bowen, R. M. (1976). Theory of mixtures. In A. C. Eringen (Ed.), *Continuum physics*, vol. III (pp. 1–127). New York: Academic Press.

Chen, C. -K., Chen, C. -H., Minkowycz, W. J., & Gill, U. S. (1992). Non-Darcian effects on mixed convection about a vertical cylinder embedded in a saturated porous medium. *International Journal of Heat and Mass Transfer*, *35*(11), 3041–3046.

Cheng, P. (1978). Heat transfer in geothermal systems. *Advances in Heat Transfer*, *14*, 1–105.

Cheng, P., & Hsu, C. T. (1986). Applications of van Driest's mixing theory to transverse thermal dispersion in forced convective flow through a packed bed. *International Communication in Heat and Mass Transfer*, *13*, 613–625.

Cheng, P., & Zhu, H. (1987). Effects of radial thermal dispersion on fully developed forced convection in cylindrical packed bed. *International Journal of Heat and Mass Transfer*, *30*(11), 2373–2383.

Combarnous, M. A., & Bories, S. A. (1975). Hydrothermal convection in saturated porous media. *Advances in Hydroscience*, *1*, 231–307.

David, E., Lauriat, G., & Prasad, V. (1989). Non-Darcy natural convection in packed-sphere beds between concentric vertical cylinders. *A.I.Ch.E. Symposium Series*, *85*(269), 90–95.

Deiber, J. A., & Bortolozzi, R. A. (1998). A two-field model for natural convection in a porous annulus at high Rayleigh numbers. *Chemical Engineering Science*, *53*, 1505–1516.

Dixon, A. G., & Cresswell, D. L. (1979). Theoretical prediction of effective heat transfer parameters in packed beds. *A.I.Ch.E. Journal*, *25*(4), 663–676.

Georgiadis, J. G., & Catton, I. (1988). An effective equation governing convective transport in porous media. *ASME Journal of Heat Transfer*, *110*, 635–641.

Glasstone, S. (1947). *Thermodynamics for chemists*. New York: Van Nostrand (Chapter 18).

Howle, L. E., & Georgiadis, J. G. (1994). Natural convection in porous media with anisotropic dispersive thermal conductivity. *International Journal of Heat and Mass Transfer*, *37*(7), 1081–1094.

Kálnay de Rivas, E. (1972). On the use of nonuniform grids in finite difference equations. *Journal of Computational Physics*, *10*, 202–210.

Kaviany, M. (1995). *Principles of heat transfer in porous media* (pp. 401–404). New York: Springer.

Kuznetsov, A. V. (1997). Thermal nonequilibrium, non-Darcian forced convection in a channel filled with a fluid saturated porous medium — a perturbation solution. *Applied Scientific Research*, *57*, 119–131.

Kuznetsov, A. V. (1998). Thermal nonequilibrium forced convection in porous media. In D. B. Ingham, & I. Pop (Eds.), *Transport phenomena in porous media* (pp. 103–129). Oxford: Pergamon-Elsevier Science.

Kunii, D., & Smith, J. M. (1960). Heat transfer characteristics of porous rocks. *A.I.Ch.E. Journal*, *6*(1), 71–78.

Martin, H. (1978). Low Peclet number particle-to-fluid heat and mass transfer in packed beds. *Chemical Engineering Science*, *33*, 913–919.

Mercer, J. W., Faust, C. R., Miller, W. J., & Pearson, F. J. (1982). Review of simulation techniques for aquifer thermal energy storage. *Advances in Hydroscience*, *13*, 1–129.

Mueller, G. E. (1991). Prediction of radial porosity distributions in randomly packed fixed beds of uniformly sized spheres in cylindrical containers. *Chemical Engineering Science*, *46*, 706–708.

Nield, D. A. (1991). Estimation of the stagnant thermal conductivity of saturated porous media. *International Journal of Heat and Mass Transfer*, *34*(6), 1575–1576.

Peaceman, D. W. (1977). *Fundamentals of numerical reservoir simulation* (pp. 37–41). Amsterdam: Elsevier.

Peirotti, M. B., Giavedoni, M. D., & Deiber, J. A. (1987). Natural convective heat transfer in a rectangular porous cavity with variable fluid properties — Validity of Boussinesq approximation. *International Journal of Heat and Mass Transfer*, *30*(12), 2571–2581.

Prasad, V., Kladias, N., Bandyopadhaya, A., & Tian, Q. (1989). Evaluation of correlations for stagnant thermal conductivity of liquid-saturated porous beds of spheres. *International Journal of Heat and Mass Transfer*, *32*(9), 1793–1796.

Prasad, V., & Kulacki, F. A. (1984). Natural convection in a vertical porous annulus. *International Journal of Heat and Mass Transfer*, *27*(2), 207–219.

Prasad, V., Kulacki, F. A., & Keyhani, M. (1985). Natural convection in porous media. *Journal of Fluid Mechanics*, *150*, 89–119.

Riaz, M. (1977). Analytical solutions for single and two-phase models of packed-bed thermal storage systems. *Journal of Heat Transfer*, *99*, 489–492.

Roache, P. J. (1972). *Computational fluid dynamics* (p. 73). Albuquerque, New Mexico: Hermosa Publishers.

Scheidegger, A. E. (1974). *The physics of flow through porous media* (pp. 197–198). Toronto: University of Toronto Press.

Spiga, G., & Spiga, M. (1981). A rigorous solution to a heat transfer two phase model in porous media and packed beds. *International Journal of Heat and Mass Transfer*, *24*, 355–364.

Stuke, B. (1948). Berechnung des wärmeaustausches in regeneratoren mit zylindrischen und kugelförmigen füllmaterial. *Angewandte Chemie*, *B20*, 262–266.

Truesdell, C. (1969). *Rational thermodynamics* (pp. 81–109). New York: McGraw-Hill.

Vafai, K. (1984). Convective flow and heat transfer in variable-porosity media. *Journal of Fluid Mechanics*, *147*, 233–259.

Vafai, K., & Kim, S. J. (1995). On the limitations of the Brinkman–Forchheimer-extended Darcy equation. *International Journal of Heat and Fluid Flow*, *16*, 11–15.

Vortmeyer, D., & Schaefer, R. J. (1974). Equivalence of the one- and two-phase models for heat transfer processes in packed beds: one dimensional theory. *Chemical Engineering Science*, *29*, 485–491.

Wakao, N., & Kaguei, S. (1982). *Heat and mass transfer in packed beds* (pp. 264–294). New York: Gordon and Breach.

Wakao, N., Kaguei, S., & Funazkri, T. (1979). Effect of fluid dispersion coefficients on particle-to-fluid heat transfer coefficients in packed beds. *Chemical Engineering Science*, *34*, 325–336.

Whitaker, S. (1986). Local thermal equilibrium: An application to packed bed catalytic reactor design. *Chemical Engineering Science*, *41*, 2029–2039.

Wong, K. F., & Dybbs, A. (1976). An experimental study of thermal equilibrium in liquid saturated porous media. *International Journal of Heat and Mass Transfer*, *19*, 234–235.